ARMA 16–769

The Interaction Analysis of Propagating Opening Mode Fractures with Veins using Discrete Element Method

Lee, H.P., Olson, J.E. and Schultz, R.A.

Department of Petroleum and Geosystems Engineering, The University of Texas at Austin, Austin, TX, USA

ABSTRACT: Veins generate mechanical discontinuities in shale formations due to their strength and stiffness contrast with the rock matrix. These heterogeneities in naturally fractured reservoirs can exert control on hydraulic fracture propagation path as demonstrated in experimental studies [1]. To investigate micromechanical fracture interaction behavior and to perform sensitivity analyses of vein properties on fracture diversion, we numerically modeled Semi-Circular Bend (SCB) tests of Marcellus shale core samples containing calcite-filled veins using the Particle Flow Code in three-dimensions (PFC3D). The numerical results correlated with experimental fracture propagation and interaction results over a range of approach angles and vein thicknesses. Further sensitivity analyses on vein properties indicated that veins with lower strength and higher stiffness contribute to more fracture diversion than veins with higher strength and lower stiffness. The vein thickness controlled the fracture travel distance inside the vein where thicker veins produced longer distance before kinking back into the rock matrix than thinner veins showing a weaker vein response. Additionally, the model showed that intergranular bond failure created microcracks within the vein as the induced fracture approached (prior to intersection), and this effect was stronger for the veins with higher stiffness relative to the rock matrix. The bond failure mode inside the vein and for the induced fracture was predominantly tensile rather than shear.

1. INTRODUCTION

Natural fractures are ubiquitous structures in the Earth's crust generated by geologic processes [2, 3]. Based on structural characterization from subsurface oil and gas reservoirs, natural fractures can range from uncemented frictional interfaces or open fractures to fully or partially cemented cohesive fractures [2, 4, 5].

Cemented natural fractures (veins) not only have resistance against shear stress but also have tensile strength [6]. These filled natural fractures can have different mechanical properties than those of the host rock [7]. The mechanical discontinuity created by the cemented natural fracture generates stress heterogeneity in the reservoir which disturbs the hydraulic fracture path.

Recently, experimental and theoretical investigations on the interaction of hydraulic fractures with bonded preexisting discontinuities have been carried out [1, 8, 9, 10, 11, 12]. Lee et al. [1] examined the interaction of a propagating fracture with calcite-filled veins in Marcellus shale core samples using the Semi-Circular Bend (SCB) test. Their results showed that fully cemented natural fractures can contribute to fracture diversion, depending on angle of approach, and the resistance of a vein to failure depends on both its fracture toughness and stiffness.

To better understand and interpret the SCB experimental results of Lee et al. [1], numerical modeling can be used. A variety of numerical models have been proposed to generate practical deformation and failure behavior of rocks. Potyondy et al. [13] discussed two methods in modeling inelastic deformation and fracture of brittle materials including rocks. One is the indirect method, where damage is represented by constitutive laws. The other is the direct method, where damage is expressed by discrete cracks.

The Discrete Element Method (DEM) is a direct method that models movements and interactions of particles [14]. Park et al. [15] noted that the direct method has several advantages over the indirect methods. For example, DEM does not require complex macroscopic constitutive relationships but directly applies Newton's second law to trace the movements and interactions of particles. Particles interact with one another through contacts or bonds, and cracks are predicted when the applied stress exceeds the tensile or shear strength of the bonds. Fractures are created by the clustering of bond breakages. Since DEM is based on microscopic mechanisms and the mode of failure is not predefined as

in continuum methods, it is ideal for investigating complex macro-mechanical behavior in heterogeneous media [16]. Another important feature of DEM is that the fracture propagation process requires no special meshing. These capabilities can contribute to understanding the interaction analysis of opening mode fractures with preexisting discontinuities.

Virgo et al. [7] investigated the interaction between preexisting veins and fractures using tension tests on notched samples with three-dimensional (3D) DEM models. They analyzed the impact of the approach angle and the strength of the vein on fracture diversion, bifurcation, and failure nucleation in the vein. In addition, Virgo et al. [17] showed that DEM can mimic the crack-seal mechanism in natural fractures. Using a two-dimensional (2D) DEM, Spence and Finch [18] studied fracture network development in reservoirs with chert nodules. They found that the influence of mechanical stratigraphy on fracture propagation created complex fracture geometries similar to those found in outcrops.

In this study, the 3D DEM technique is introduced to investigate micromechanical fracture interaction behavior observed in the SCB experiments of Lee et al. [1].

2. PARTICLE FLOW CODE

The Particle Flow Code in three-dimensions (PFC3D) [19] is also known as a Bonded-Particle Model (BPM) that directly mimics the behavior of rocks. It uses three main components: particles, bonds, and walls. Particles consist of mass and volume, and they are used to represent grains, clusters of grains, or larger solid elements. Adjacent particles are held together with bonds, which can resist moment or rotation. Particles and bonds work together to form a densely packed assembly representing a rock specimen. Walls act as the boundary for sample generation and as the loading surface for inducing deformation. Contacts, cracks, and positions of particles are calculated every time step.

3. SAMPLE ASSEMBLY

3.1. Sample Assembly Generation

The procedure for generating a sample assembly in PFC3D is outlined in Potyondy and Cundall [20] and Park et al. [15]. Three cylindrical walls (one above and two below the specimen) represented the loading and supporting rollers. Fig. 1 shows the comparison between the SCB test in the laboratory and in PFC3D. Particles and parallel bonds representing the vein were grouped together and assigned with a different set of microscopic properties compared to the rock matrix.

3.2. Microscopic Parameter Determination

The total number of particles in DEM governs the overall computational time, and it is typically impractical to set a particle to express one grain. Assuming a grain size in shale of less than 0.004 mm in diameter would require billions of particles to describe a single SCB specimen of the Marcellus shale [1]. Thus, the particles in this study are discrete solid elements, representing clusters of grains, and these elements are bonded together to make the whole sample.

A distribution of particle sizes is used to get a dense pack of elements, with the minimum particle diameter (D_{min}) of 0.45 mm and D_{max}/D_{min} of 1.65 [20]. The average diameter of particles is chosen to be small relative to sample size, on the order of a few percent or less of the specimen diameter. Further analysis on the effect of particle size to sample size ratio is not

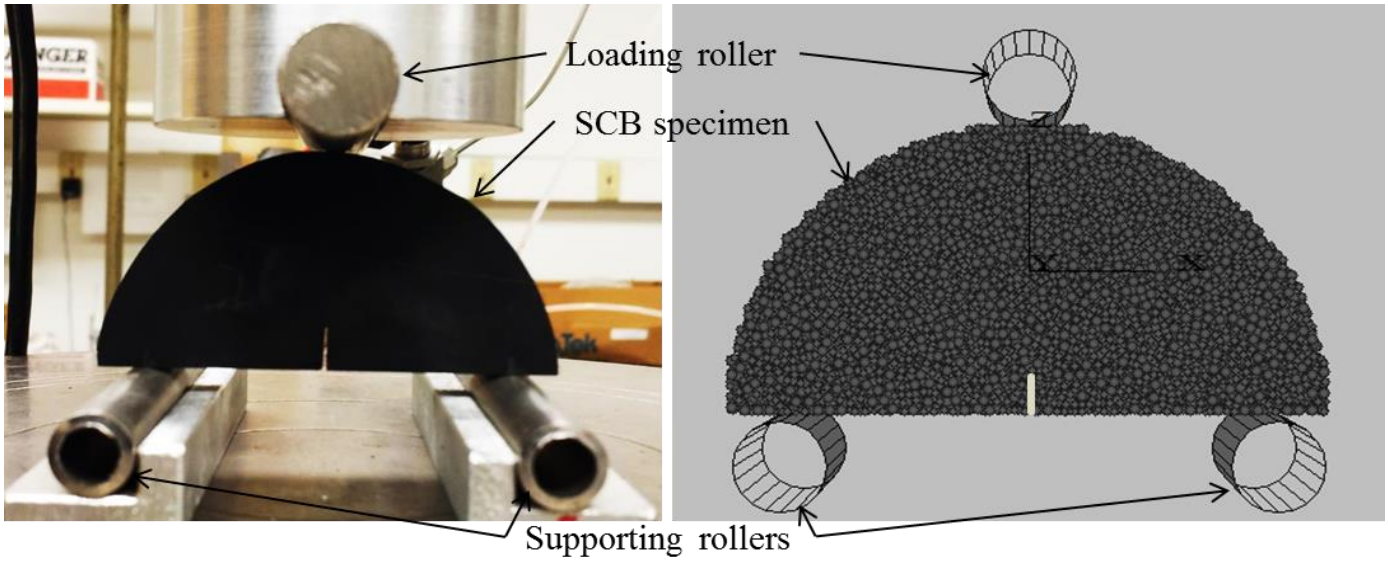

Fig. 1. The experimental set-up of SCB test (left) and the numerically modeled SCB test with PFC3D (right).

discussed in this paper but other work [21] shows that the assigned particle distribution provides representative results to evaluate the interaction between fracture and preexisting discontinuity.

To match the input microscopic properties of particles and bonds to the measured rock mechanical properties (e.g., Young's modulus, E; Possion's ratio, v; Uniaxial Compressive Strength, UCS; Tensile strength, σ_t), it is necessary to carry out a trial-and-error process with conventional experimental tests in PFC3D, such as the Brazilian test, the uniaxial and the triaxial compression test. Macroscopic mechanical properties of Marcellus core samples (E^{rock} of 8.9 GPa and UCS^{rock} of 53.4 MPa) [1] and published log data (v^{rock} of 0.25–0.3) [22, 23] are utilized to determine microscopic properties of the particles and parallel bonds (Table 1).

It is worth noting that several studies have found that PFC3D usually predicts higher tensile strength compared to experiments and it is difficult to match both UCS and σ_t for a given sample using one set of input properties [20, 24]. Park et al. [15] noted σ_t appears to depend more on the sample size than does UCS. Therefore, microproperties are matched with the lowest UCS value of the experimental range and the interaction analysis will not focus so much on an exact quantitative value but mostly on the relative fracture toughness between the rock and the vein.

Table 1. The elastic properties and strengths of Marcellus shale in experiment and PFC3D

Properties	Experiment	PFC3D
E (GPa)	8.9 ± 0.17	8.93
UCS (MPa)	53.4 ± 8.6	46.4
K_{Ic} (MPa$\sqrt{m}$)	0.64 ± 0.17	1.08
	Literature	PFC3D
v	0.25–0.3	0.277

Table 2. Microproperties for the rock matrix in PFC3D

Particle properties	
Modulus, E_c (GPa)	11.0
Normal/Shear Stiffness Ratio, k_n/k_s	2.5
Min. Particle Diameter, D_{min} (mm)	0.45
Max./Min. Diameter Ratio, D_{max}/D_{min}	1.65
Friction Coefficient, μ	0.75
Density, ρ (kg/m^3)	2650
Parallel bond properties	
Modulus, E_p (GPa)	11.0
Normal/Shear Stiffness Ratio, k_{np}/k_{sp}	2.5
Normal Strength, σ_p (MPa)	45.0 ± 4.5
Shear Strength, τ_p (MPa)	45.0 ± 4.5
Radius Multiplier, λ_p	0.9

After the calibration, microscopic input parameters for the rock matrix are determined as listed in Table 2. The friction coefficient (μ) was assumed to be 0.75, a value within the range of μ for rocks, 0.6 to 0.85 [25].

3.3. SCB SPECIMEN WITH VEIN

The mechanical properties of the calcite vein are different from the shale matrix. They disturb the stress field in the specimen, introducing difficulties in the analytical prediction of fracture crossing or diversion. The main objective of the numerical analysis is to understand the mechanisms and important factors in the interaction between the propagating fracture and the vein, examining a wider range of conditions than possible using a limited number of samples available for laboratory SCB testing. In the PFC3D model, calcite veins were implemented with various approach angles, strengths, thicknesses, and stiffness ratios to the rock matrix to perform sensitivity analysis on each constituent.

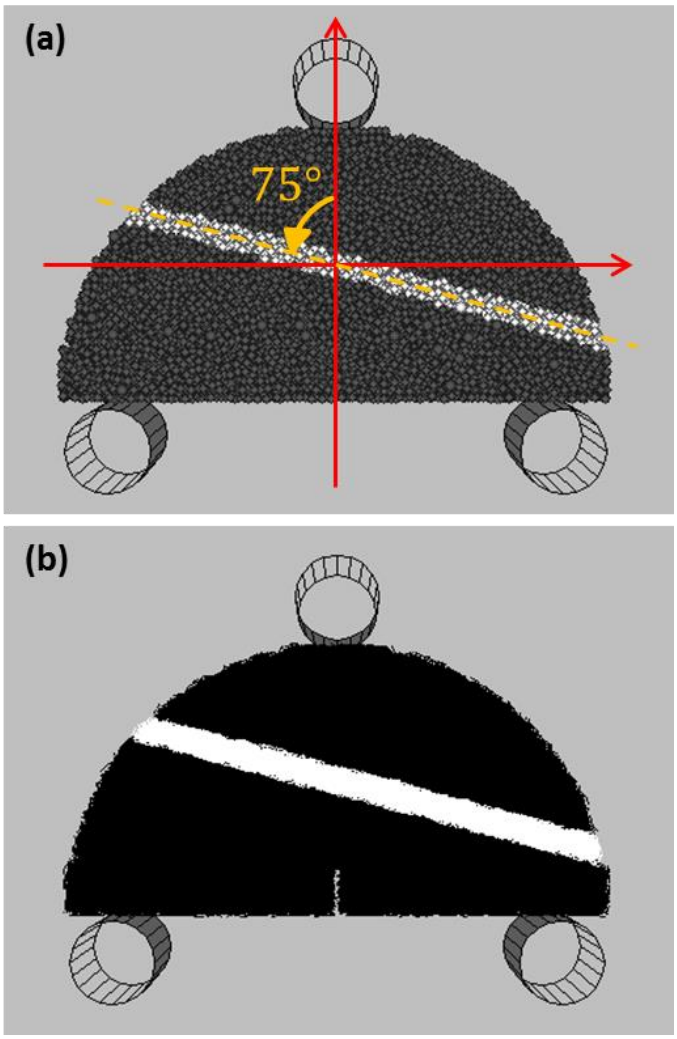

Fig. 2. Schematic views of SCB test set-up in PFC3D: (a) particles representing shale matrix (dark gray) with a vein (white) at 75° and (b) parallel bonds of the rock matrix (black) and the vein (white).

Following the steps described in Section 3.1, a SCB test specimen was made ready for loading as shown in Fig. 2. The diameter of the modeled sample is 58.4 mm (2.3 inch), and the thickness is 14 mm (0.55 inch) for all cases. The sample is comprised of 19,697 particles and 54,544 parallel bonds. Dark gray particles represent shale matrix and white particles compose the calcite-cemented vein (Fig. 2a). The notch at the bottom of the sample is created by deleting the parallel bonds at that location (Fig. 2b).

The particle size used for the sample constrained the minimum vein thickness. In order for the vein to have independent properties from the shale matrix, the vein thickness had to be at least two times the maximum particle diameter ($2D_{max}$=1.485 mm). Otherwise a vein particle could be bonded to matrix particles on both sides of the vein. Given the variability of random packing and particle contacts, however, it was found that for practical reasons, the minimum vein thickness achievable was 1.9 mm. This is the thickest vein case examined in the Marcellus shale experiments [1].

The microscopic properties of the vein, the stiffness and strength of the parallel bonds and the stiffnesses of particles, were set as ratios of the rock matrix values. To represent weaker and stiffer veins in the rock matrix, the parallel bond strengths were set between 0.5 and 1.0 times the strength of the shale and the stiffnesses were varied between 1 and 10 times the shale. The bond strength of the matrix-vein interface was set to match the bond strength of the rock matrix because our laboratory experiments [1] indicated failure always occurred within the vein calcite.

4. RESULTS

4.1. Influence of Approach Angle on Fracture Path

The approach angle is an important factor that governs the fracture interaction result [1, 8, 10, 12, 26]. In our naturally fractured Marcellus shale experiments [1], the core samples only offered a limited range of approach angle for certain vein thicknesses. In the PFC3D modeling, we used an increment of 15° for vein approach angle for a wide range of vein thicknesses, strengths and stiffnesses.

One important thing in the energy release rate criterion is the consideration of the vein stiffness in estimating the critical strength of the preexisting discontinuity [9]. Such inclusions are generally not considered in other fracture interaction analyses [10, 27, 28, 29]. To examine if the vein stiffness has impact on the vein to act as a plane of weakness in the fracture-interaction process, the samples include veins of parallel bond strength the same as that of the rock matrix ($1{\cdot}K_{Ic}^{rock}$) but ten times the stiffness ($10{\cdot}E^{*rock}$), where $E^{*}= E/(1–\nu)$ is the plane modulus. The critical energy release rate of the vein (G_c^{vein}) can be expressed as [30]

$$G_c^{vein} = \frac{\left(K_{Ic}^{vein}\right)^2}{E^{*vein}} = 0.1\frac{\left(K_{Ic}^{rock}\right)^2}{E^{*rock}} = 0.1\times G_c^{rock}. \quad (1)$$

Parallel bond breakages in PFC3D results are marked with green for tensile failure and magenta for shear mode failures (Fig. 3). Scattered parallel bond breakages indicate microcracks and cluster of breakages that are continuous is interpreted as the propagating fracture.

In Fig. 3, the fracture diverted into the vein for approach angles of 60° and lower. Although the vein fracture toughness is same as the rock matrix, veins with higher stiffness show a weaker vein response and contribute to more fracture diversion. When the fracture crossed the vein, the propagating fracture left vein-parallel damage and the damage extended to both wings of the vein. Regardless of the fracture crossing-versus-diversion results, the failure mode of the fracture mostly indicated tensile mode (green marks) both in the vein and rock matrix rather than shear breakages (magenta marks) for all cases.

However, the fracture did not divert into the fracture starting from the approach angle of 90°, as was predicted by the energy release rate criterion [1]. This discrepancy may arise from the fact that, in PFC3D, there were no internal flaws or weak planes in the vein that could be utilized to divert the fracture. Despite the mismatching quantitative values, fracture diversion was likely to occur more in the lower approach angles than the in higher angles following the trend of the experimental fracture interaction response.

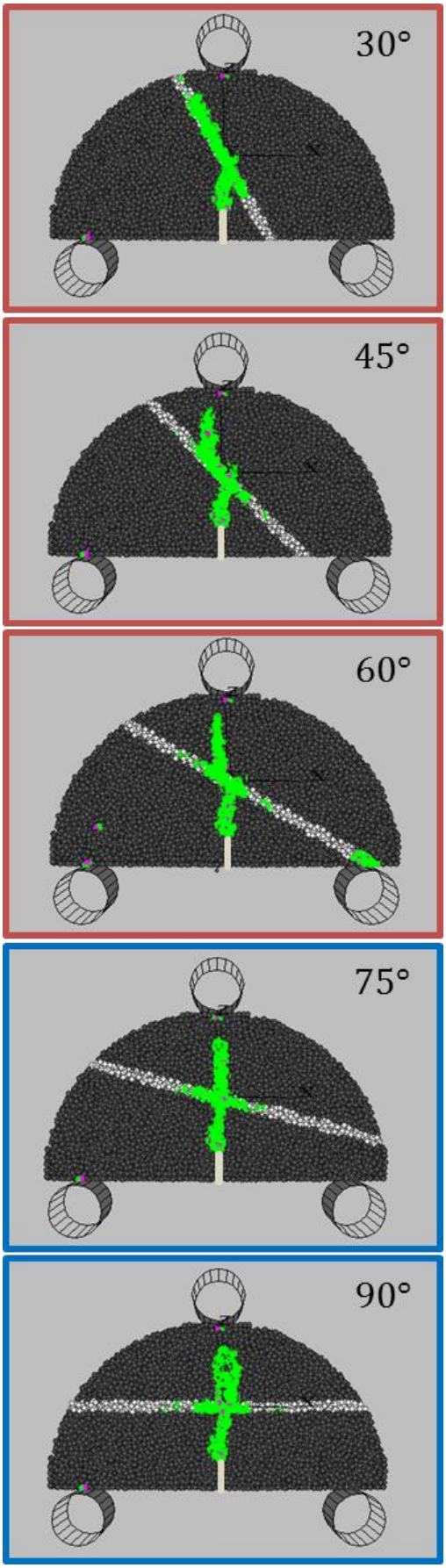

Fig. 3. SCB test results with veins ($1{\cdot}K_{Ic}^{rock}$ and $10{\cdot}E^{*rock}$) at approach angles of 30°, 45°, 60°, 75°, and 90°. Red and blue boxes indicate fracture diversion and fracture crossing, respectively.

Fig. 4 illustrates the fracture propagation process in the SCB test with the corresponding load-displacement curve for the SCB specimen with a vein at an approach angle of 30° (from Fig. 3). At the peak load, tensile cracks were generated from the notch tip (Fig. 4a) and the fracture started to propagate. Microcracks were generated inside the vein before the fracture, initiating from the notch tip, encountered the vein. When the opening mode fracture approached the vein, it utilized the induced microcracks and diverted into the vein (Fig. 4b). After the interaction, the induced fracture propagated within the vein while the load dropped continuously (from Fig. 4b to Fig. 4d). The failure behavior of the sample was very brittle as the load dropped down to 100 N abruptly and the interaction between the opening mode fracture and the vein occurred instantaneously after the peak load (Fig. 4e).

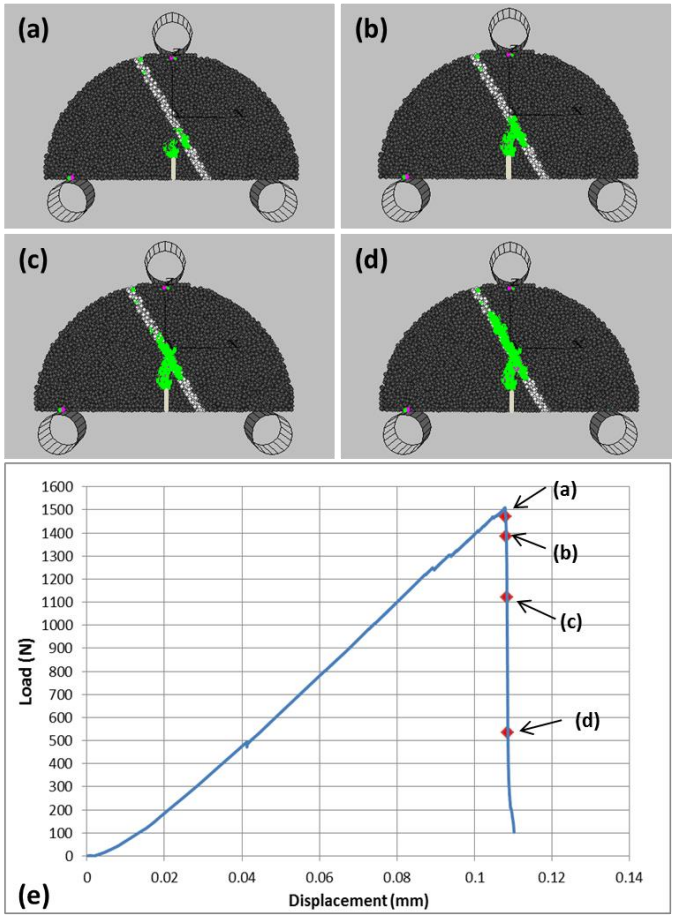

Fig. 4. Fracture propagation process in the PFC3D specimen with a vein ($1{\cdot}K_{Ic}^{rock}$ and $10{\cdot}E^{*rock}$) at an approach angle of 30°. Figures (a) to (d) correspond to the points marked in the (e) load–displacement curve measured from the loading roller.

4.2. *Influence of Vein Stiffness on Fracture Path*

In order to examine the stiffness effect specifically, the study performed SCB tests on samples with veins at 60° with three different E^{*vein} ($1{\cdot}E^{*rock}$, $5{\cdot}E^{*rock}$, $10{\cdot}E^{*rock}$) and a constant parallel bond strength ($0.5{\cdot}K_{Ic}{}^{rock}$). The fracture in Fig. 5a and Fig. 5b both diverted into the vein but the fracture propagated along the vein with a longer distance for the vein with a higher stiffness (Fig. 5b). This is because higher E^{*vein} generates higher stress in the vein than in the shale, causing the vein to act more like a weaker plane. Furthermore, the case of $10{\cdot}E^{*rock}$ (Fig. 5c) failed through the vein even before the fracture from the notch tip reached the vein.

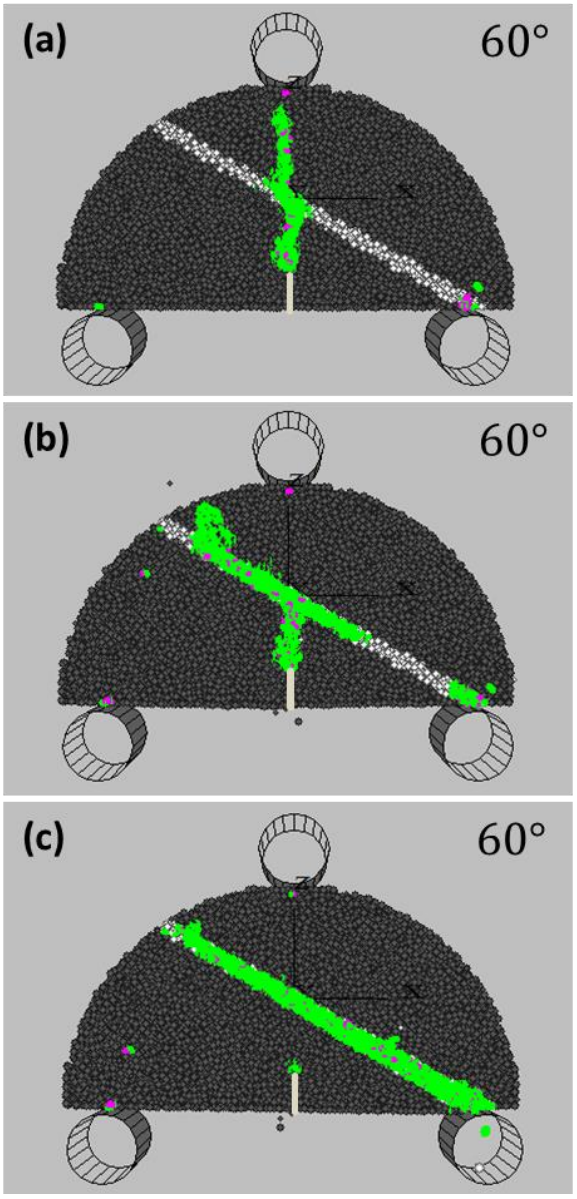

Fig. 5. SCB results of veins at 60° with three stiffnesses: E^{*vein} of (a) $1{\cdot}E^{*rock}$, (b) $5{\cdot}E^{*rock}$, and (c) $10{\cdot}E^{*rock}$. The fracture toughness of the vein is kept constant with 0.5 ratio to the rock fracture toughness ($0.5{\cdot}K_{Ic}{}^{rock}$) for all three cases.

4.3. *Influence of Vein Thickness on Fracture Path*

The effect of vein thickness on the fracture interaction is assessed numerically to further explore the experimental results [1]. In general, as the relative stiffness of the vein to the rock increases, a stress concentration develops in the vein which can lead to the failure of the weak plane as observed in Fig. 4. It is important to examine if the incremental growth of the vein thickness amplifies this effect, which can eventually influence the fracture interaction behavior. Therefore, the SCB test was used to examine specimens with three different vein thicknesses (1.9 mm, 2.5 mm, 3.2 mm). The samples contained veins with a stiffness of $5{\cdot}E^{*rock}$ and strength of $0.5{\cdot}K_{Ic}{}^{rock}$ at an approach angle of 90° (Fig. 6).

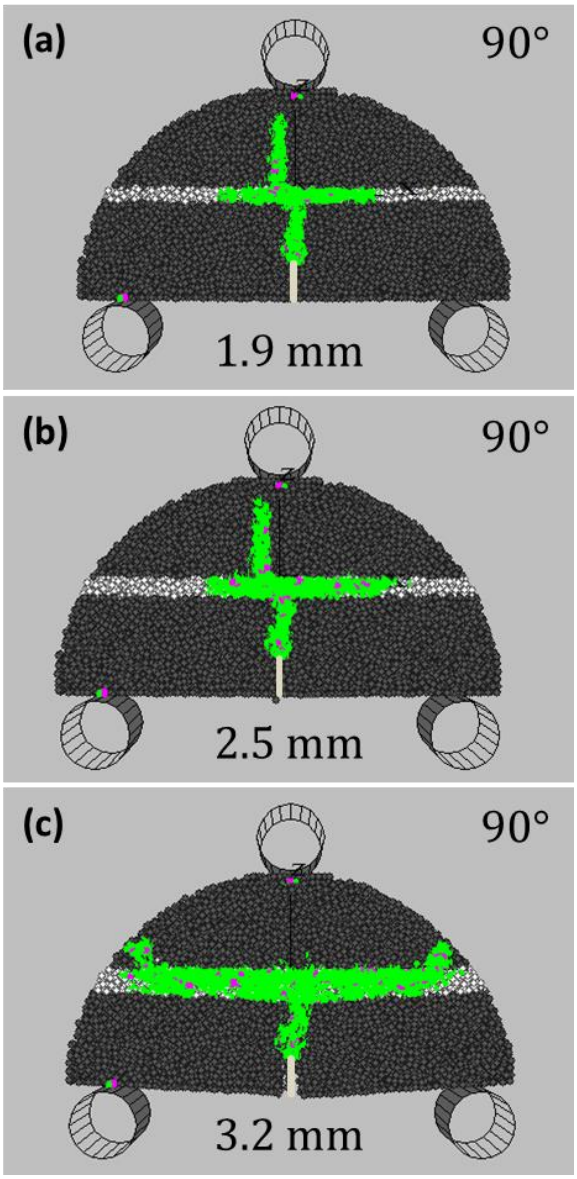

Fig. 6. SCB results of veins at 90° with three thicknesses: (a) 1.9 mm, (b) 2.5 mm, (c) 3.2 mm. For all samples, the vein stiffness is 5 times greater than the rock matrix ($5{\cdot}E^{*rock}$) and the fracture toughness is 0.5 ratio ($0.5{\cdot}K_{Ic}{}^{rock}$) to the rock matrix.

The SCB results from PFC3D show that for the thickest vein sample (Fig. 6c – 3.2 mm) the induced fracture diverted into the vein and propagated almost to the end of the sample before it kinked back into the rock matrix, presumably due to the compressive stress concentration generated by the three-point bending load. However, the propagating fracture of the two other samples with thinner veins (Fig. 6a – 1.9 mm and Fig. 6b – 2.5 mm) kinked back into the rock matrix closer to the point of the initial deflection without promoting the total breakage of the vein. Despite the same G_c^{vein} for all three samples, the fracture traveled in the vein for a longer distance as the vein thickness became larger.

5. CONCLUSIONS

Numerical analysis of fracture propagation in SCB tests provides a better understanding of the influence of vein properties on fracture-fracture interactions. Numerical SCB test results qualitatively matched with the fracture diversion results of the physical experiments [1] and other numerical results [7]. Propagating tensile fractures were more likely to divert into pre-existing veins for lower approach angles. Fracture diversion was more likely to occur for the samples of veins with higher stiffness or lower strength, which confirmed that the critical energy release rate is a more robust parameter for predicting failure in fracture interaction cases than fracture toughness or tensile strength alone. Samples with thicker veins showed a weaker response than those with thinner veins, which agrees with the SCB results on hydrostone with inclusions [12].

As the opening mode fracture approached the vein, microcracks were generated inside the vein even before the fracture intersected it. When the opening mode fracture diverted into the vein, it utilized the microcracks to propagate along the vein but some fractures, especially for samples with high approach angles, crossed the vein regardless the locations of microcrack damage in the vein. All of the fractures in PFC3D, including both fractures that crossed and diverted, propagated continuously without jumping across the vein and initiating on the other side of the rock matrix. The failure mode of the parallel bonds in the vein during the fracture interaction process was mostly tensile rather than shear failure.

The results of this study illustrate fracture interaction mechanics that can be applied to the prediction of hydraulic fracture geometry in naturally fractured reservoir rocks.

ACKNOWLEDGEMENTS

We give special thanks to ExxonMobil for its funding and Pennsylvania General Energy (PGE) for its acquisition of the Marcellus core that was utilized in this study and their permission to publish the results.

REFERENCES

1. Lee, H.P., J.E. Olson, J. Holder, J.F.W. Gale, and R.D. Myers. 2015. The interaction of propagating opening mode fractures with preexisting discontinuities in shale. *J. Geophys. Res.* 120, 1: 169–181.
2. Ramsay, J.G. 1980. The crack-seal mechanism of rock deformation. *Nature* 284, 5752: 135–139.
3. Engelder, T. 1987. Joints and shear fractures in rock. In *Fracture mechanics of rock*, ed. B.K. Atkinson, London, England, Academic Press, 27–69.
4. Laubach, S.E. 2003. Practical approaches to identifying sealed and open fractures. *AAPG Bulletin* 87, 4: 561–579.
5. Gale, J.F.W., S.E. Laubach, J.E. Olson, P. Eichhubl, and A. Fall. 2014. Natural fractures in shale: A review and new observations. *AAPG Bulletin* 98, 11: 2165–2216.
6. Caputo, R. 2010. Why joints are more abundant than faults: A conceptual model to estimate their ratio in layered carbonate rocks. *J. Struct. Geol.* 32: 1,257–1,270.
7. Virgo, S., S. Abe, and J.L. Urai. 2013. Extension fracture propagation in rocks with veins: Insight into the crack-seal process using Discrete Element Method modeling. *J. Geophys. Res.* 118, 10: 5,236–5,251.
8. Zhou, J., M. Chen, Y. Jin, and G. Zhang. 2008. Analysis of fracture propagation behavior and fracture geometry using a tri-axial fracturing system in naturally fractured reservoirs. *Int. J. Rock Mech. Min. Sci.* 45, 7: 1,143–1,152.
9. Dahi-Taleghani, A. and J.E. Olson. 2009. Numerical modeling of multi-stranded hydraulic fracture propagation: accounting for the interaction between induced and natural fractures. *SPE J.* 16, 3: 575–581.
10. Gu, H. and X. Weng. 2010. Criterion for fractures crossing frictional interfaces at non-orthogonal angles. In *Proceedings of the 44th U.S. Rock Mechanics Symposium and 5th U.S.-Canada Rock Mechanics Symposium, Salt Lake City, Utah, 27–30 June 2004*, ARMA 10–198.
11. Bahorich, B.L., J.E. Olson, and J. Holder. 2012. Examining the effect of cemented natural fractures on hydraulic fracture propagation in hydrostone block experiments. In *Proceedings of the SPE Annual Technical Conference and Exhibition, San Antonio Texas, 8–10 October 2012*, SPE 160197.

12. Wang, W., J.E. Olson, and M. Prodanović. 2013. Natural and hydraulic fracture interaction study based on semi-circular bending experiments. In *Proceedings of the Unconventional Resources Technology Conference, Denver, Colorado, 12–14 August 2013*, SPE 168714/URTeC 1576910.

13. Potyondy, D.O., P.A. Cundall, and C.A. Lee. 1996. Modelling rock using bonded assemblies of circular particles. In *Rock Mechanics*, eds. M. Aubertin, F. Hassani, H. Mitri, 1,937–19,44.

14. Cundall, P.A. and O.D.L. Strack. 1979. A discrete numerical model for granular assemblies. *Géotechnique* 29, 1: 47–65.

15. Park, N., J. Holder, and J.E. Olson. 2004. Discrete element modeling of fracture toughness tests in weakly cemented sandstone. In *Proceedings of the 6th North America Rock Mechanics Symposium (NARMS), Houston, Texas, 5–9 June 2004*, ARMA/NARMS 04–553.

16. Schöpfer, M.P.J., S. Abe, C. Childs, and J.J. Walsh. 2009. The impact of porosity and crack density on the elasticity, strength and friction of cohesive granular materials: Insights from DEM modelling. *Int. J. Rock Mech. Min. Sci.* 46: 250–261.

17. Virgo, S., S. Abe, and J.L. Urai. 2014. The evolution of crack seal vein and fracture networks in an evolving stress field: Insights from Discrete Element Models of fracture sealing. *J. Geophys. Res.* 119, 12: 8708–8727.

18. Spence, G.H. and E. Finch. 2014. Influences of nodular chert rhythmites on natural fracture networks in carbonates: An outcrop and two-dimensional discrete element modelling study. In *Advances in the Study of Fractured Reservoirs*, eds. G.H Spence, J. Redfern, R. Aguilera, T.G. Bevan, J.W. Cosgrove, G.D. Couples, J.M. Daniel, Geological Society, London, Special Publications 374: 211–249

19. Itasca Consulting Group, Inc. 2008. Particle Flow Code in 3 Dimensions (PFC3D) Manual, Version 4.0.

20. Potyondy, D.O. and P.A. Cundall. 2004. A bonded-particle model for rock. *Int. J. Rock Mech. Min. Sci.* 41: 1,329–1,364.

21. Lee, H.P. 2015. Fracture propagation in naturally fractured reservoirs. *PhD Dissertation*, The University of Texas at Austin, Austin, Texas, USA.

22. Gargouri, M. 2012. Multicomponent 3D seismic interpretation of the Marcellus Shale Bradford County, Pennsylvania. *MS Thesis*, University of Houston, Houston, Texas, USA.

23. Izadi, G., J. Junca, C. Cade, and T. Rowan. 2014. Multidisciplinary study of hydraulic fracturing in the Marcellus shale. In *Proceedings of the 48th US Rock Mechanics / Geomechanics Symposium, Minneapolis, MN, USA, 1–4 June 2014*, ARMA 14–6975.

24. Park, N. 2006. Discrete element modeling of rock fracture behavior: Fracture toughness and time-dependent. *PhD Dissertation*, The University of Texas at Austin, Austin, Texas, USA.

25. Byerlee, J. 1978. Friction of rocks. *Pure Appl. Geophys.* 116, 4–5: 615–626.

26. Blanton, T.L. 1982. An experimental study of interaction between hydraulically induced and pre-existing fractures. In *Proceedings of the SPE/DOE Unconventional Gas Recovery Symposium, Pittsburgh, PA, 16–18 May 1982*, SPE/DOE 10847.

27. Blanton, T.L. 1986. Propagation of hydraulically and dynamically induced fractures in naturally fractured reservoirs, In *Proceedings of the Unconventional Gas Technology Symposium, Louisville, KY, 18–21 May 1986*, SPE 15261.

28. Warpinski, N.R. and L.F. Teufel. 1987. Influence of geological discontinuities on hydraulic fracture propagation. *J. Petrol. Tech.* 39, 2: 209–220.

29. Renshaw, C.E. and D.D. Pollard. 1995. An experimentally verified criterion for propagation across unbounded frictional interfaces in brittle, linear elastic materials. *Int. J. Rock Mech. Min. Sci. Geomech. Abstr.* 32, 3: 237–249.

30. Lawn, B.R. and T.R. Wilshaw. 1975. *Fracture of brittle solids.* Cambridge University Press, Cambridge.